Accurate critical pressures for structural phase transitions of group IV, III-V, and II-VI compounds from the SCAN density functional

Chandra Shahi,[1,*] Jianwei Sun,[2] and John P. Perdew[3]

[1]*Department of Physics, Temple University, Philadelphia, Pennsylvania 19122, USA*

[2]*Department of Physics and Engineering Physics, Tulane University, New Orleans, Louisiana 70118, USA*

[3]*Departments of Physics and Chemistry, Temple University, Philadelphia, Pennsylvania 19122, USA*

(Received 7 November 2017; revised manuscript received 15 January 2018; published 26 March 2018)

Most of the group IV, III-V, and II-VI compounds crystallize in semiconductor structures under ambient conditions. Upon application of pressure, they undergo structural phase transitions to more closely packed structures, sometimes metallic phases. We have performed density functional calculations using projector augmented wave (PAW) pseudopotentials to determine the transition pressures for these transitions within the local density approximation (LDA), the Perdew-Burke-Ernzerhof (PBE) generalized gradient approximation (GGA), and the strongly constrained and appropriately normed (SCAN) meta-GGA. LDA underestimates the transition pressure for most of the studied materials. PBE under- or overestimates in many cases. SCAN typically corrects the errors of LDA and PBE for the transition pressure. The accuracy of SCAN is comparable to that of computationally expensive methods like the hybrid functional HSE06, the random phase approximation (RPA), and quantum Monte Carlo (QMC), in cases where calculations with these methods have been reported, but at a more modest computational cost. The improvement from LDA to PBE to SCAN is especially clearcut and dramatic for covalent semiconductor-metal transitions, as for Si and Ge, where it reflects the increasing relative stabilization of the covalent semiconducting phases under increasing functional sophistication.

DOI: 10.1103/PhysRevB.97.094111

I. INTRODUCTION

The experimental study of pressure-induced structural phase transitions of group IV, III-V, and II-VI compounds began in the early 1960s. Much progress has been made with advances in measurement methods. However, it is quite challenging to find an accurate equilibrium transition pressure (the pressure at which both phases can coexist in equilibrium) experimentally. Hysteresis due to an energy barrier is common in a first-order phase transition, making it hard to locate the transition point. Also, the transition pressure may be sensitive to the measurement method, sample type, and nonhydrostatic stress condition.

The structural phase transition of solids also poses a considerable challenge to theoretical models. The high-pressure phases of these materials using density functional calculation within the local density approximation (LDA) have been reviewed by Mujica *et al.* [1]. LDA underestimates the transition pressure for the first transition of a series under increasing pressure. Most of the first transitions are reconstructive, and the initial phases are semiconducting. The semiconductor-metal (diamond $\rightarrow$ β-tin) transition for Si is the most studied: Hennig *et al.* [2] have shown that LDA and GGA functionals underestimate the transition pressure. Older meta-GGAs predict a less accurate transition pressure than GGA does [3,4]. However, the hybrid functional HSE06, the random phase approximation (RPA), and diffusion Monte Carlo (DMC) predict the transition pressure in agreement with experiment, but at an increased computational cost. The recent meta-GGA SCAN [5], on the other hand, yields an accurate prediction for Si [6] at a GGA-like cost, suggesting that SCAN is a promising functional for the study of structural transition. In this paper, we calculate the transition pressure for group IV, III-V, and II-VI materials using SCAN as well as LDA and PBE.

The critical pressure of a structural phase transition is a sensitive test of an approximate density functional, because it depends upon a small change of total energy arising from a large change of electron density [4]. By contrast, the lattice constant for a given structure is relatively much more accurate, even in the simplest density functional approximation, because it depends upon a small change of energy arising from a small change of electron density [4].

In ground-state density functional theory (DFT) [7,8], the density functional for the exchange-correlation energy $E_{\rm XC}$ is the only needed approximation. Jacob's ladder [9] is often used to order the approximate functionals, in which higher rungs are potentially more sophisticated and accurate. The first three rungs of approximations can be described by the formula

$$E_{\rm XC}[n_\uparrow,n_\downarrow] = \int n\varepsilon_{\rm XC}(n_\uparrow,n_\downarrow,\nabla n_\uparrow,\nabla n_\downarrow,\tau_\uparrow,\tau_\downarrow)\,d^3r. \quad (1)$$

Here $n = n_\uparrow + n_\downarrow$ is the total electron density. ∇n_σ is the spin-density gradient, and $\tau_\sigma = \Sigma_i^{\rm occ}\frac{1}{2}|\nabla\psi_{i,\sigma}|^2$ is the orbital kinetic density for Kohn-Sham orbitals $\psi_{i,\sigma}$ of spin σ.

Equation (1) represents the local spin density approximation (LSDA) [7], the first rung of Jacob's ladder, if the spin densities n_σ are the only ingredients of the exchange-correlation energy per particle $\varepsilon_{\rm xc}(\vec{r})$. In this approximation, a general nonuniform electron gas is considered locally uniform. The

*schandra@temple.edu

exchange-correlation energy for a uniform gas is well known. Therefore, the LSDA is exact for a uniform gas and accurate for very slowly varying spin densities. It is expected to work for simple metals, but it works better than it was expected to work for atoms and molecules, in which the electron density is far from homogeneous. Since LSDA overly favors homogeneity, it overestimates the cohesive energy of molecules and solids and underestimates bond length and lattice constant.

The second rung of Jacob's ladder is the generalized gradient approximation (GGA), in which spin densities and their gradients at a point are the ingredients of ε_{xc}. The Perdew-Burke-Ernzerhof (PBE) [10] is a popular GGA functional. It is constructed to satisfy 11 known exact constraints on the exchange-correlation energy functional. PBE favors inhomogeneity more than the LDA does. It underestimates the cohesive energy and overestimates the lattice constant of a solid.

The third rung of Jacob's ladder is the meta-GGA. The strongly constrained and appropriately normed (SCAN) [5] functional is a new meta-GGA, designed to satisfy all 17 known exact constraints that a semilocal functional can. In SCAN, the exchange-correlation energy per particle ε_{xc} for a spin-unpolarized density depends on the orbital kinetic densities only via the dimensionless variable

$$\alpha = (\tau - \tau^w)/\tau^{\text{unif}}.$$

Here $\tau^w = |\nabla n|^2/8n$ is the von Weizsäcker kinetic energy density, which is exact for any system with a single orbital shape, and $\tau^{\text{unif}} = (3/10)(3\pi^2)^{2/3}n^{5/3}$ is the Thomas-Fermi uniform density limit. Without being fitted to any bonded system, SCAN accurately [6] describes materials with different types of bonding: covalent (characterized by $\alpha \approx 0$ for single bonds), metallic ($\alpha \approx 1$), and weak ($\alpha \gg 1$). SCAN provides a different and appropriate GGA description in each of these three limits or bonding situations [11]. The satisfaction of many universal constraints (bounds, scaling relations, limits, etc.) makes SCAN more predictive than GGAs or meta-GGAs that satisfy fewer exact constraints. At a computational cost at most only a few times greater than that of PBE, SCAN meets many condensed-matter challenges: ferroelectrics [12,13], metal surfaces [14], formation energies [15], structure prediction [15], liquid water [16], and liquid silicon [17].

II. COMPUTATIONAL METHOD

We performed density functional calculations for energy per unit cell as a function of cell volume with the VASP [18,19] code (Vienna ab initio simulation package). VASP uses the projector augmented wave (PAW) method and a plane-wave basis set. Scalar relativistic effects are included via the PAW pseudopotential. For elements from the fourth row and further down the periodic table, semicore d electrons are considered as valence electrons, with the exception of Sb, Se, and Te, in which only outermost s and p electrons are considered as valence. Three levels of functional approximation were used: the Ceperley-Alder LDA [20] as parametrized by Perdew and Zunger [21], the Perdew-Burke-Ernzerhof (PBE) [10] GGA, and the SCAN [5] meta-GGA. The integration grids (k mesh) over the Brillouin zone were generated by the Γ-centered method. The total energy was converged to 1 meV per atom with respect to the energy cutoff and the k mesh. In the structural optimization, the forces on the atoms were below 0.01 eV Å^{-1}. The kinetic energy cutoff for the plane wave expansion and the k-mesh size are provided in the Supplemental Material [22].

To calculate the transition pressure, we used the fact that the Gibbs free energies G (which reduce in our calculations to enthalpies at zero temperature) per formula unit of the two competing crystallographic phases with the same chemical formula must be equal at phase equilibrium under conditions of constant pressure and temperature. Our approach is formally equivalent to finding the equilibrium transition pressure as minus the slope of the common tangent to the binding energy curves of the two phases, but in practice our approach is numerically simpler and thus more accurate. Using the Murnaghan equation of state [23], enthalpy as a function of pressure can be expressed as

$$\begin{aligned} H(P) &= E + PV \\ &= E_0 + \frac{B_0 V_0}{B_0' - 1}\left[\left(1 + \frac{B_0'}{B_0}P\right)^{(B_0'-1)/B_0'} - 1\right]. \end{aligned}$$

Here E_0 and V_0 are the equilibrium energy and volume per formula unit, while B_0 and B_0' are the bulk modulus and pressure derivative of the bulk modulus at zero pressure. These parameters, extracted from our calculated energy as a function of cell volume for each considered solid phase and functional, are reported in the Supplemental Material [22], along with the fitting range for the equation of state.

III. RESULTS AND DISCUSSIONS

Our results are presented in Tables I–III and discussed below.

A. Si and Ge

Si and Ge crystallize in the tetrahedrally bonded diamond structure at ambient conditions. The first high-pressure phase is a tetragonal β-tin phase. For these transitions, Gaál-Nagy *et al.* [35] have shown that the zero-point energy (ZPE) and the finite-temperature (300 K) phonon correction lower the transition pressure by 1.3 GPa.

Si undergoes this semiconductor-metal transition at 11.2–12.6 GPa [24]. With the ZPE and the finite-temperature correction [35] included, we find the transition pressure to be 5.8 GPa with LDA, 8.5 GPa with PBE, and 13.2 GPa with SCAN. LDA and PBE underestimate the transition pressure; this is in accord with previous studies [2,3]. In fact, it was the serious underestimation [3,4] by our earlier TPSS meta-GGA that provided the initial motivation to develop SCAN. The SCAN result is in good agreement with experimental results. It agrees with the high-level approximations HSE06 (13.3 GPa) [4] and RPA (12.2 GPa) [4]. However, it is also important to compare the result with a more accurate method like quantum Monte Carlo (QMC). Our SCAN transition pressure is in perfect agreement with the DMC result of (14 ± 1) GPa [2]. This is because the SCAN energy difference (417 meV/atom) is in agreement with the DMC result (424 ± 20 meV/atom). SCAN predicts an accurate energy difference of the two phases in Si because it can distinguish the covalent and metallic

TABLE I. The calculated equilibrium transition pressure (in GPa) for the group IV materials within the LDA, PBE, and SCAN XC functionals. ZPE and vibrational effects are not included in the calculated value. The experimental pressure (in GPa) to the right of the vertical bar corresponds to the forward transition and the left one to the reverse transition.

	LDA	PBE	SCAN	Other works	Expt.
Si (diamond→ β-tin)	7.1	9.8	14.5	3.5 – 10[f], 12.2[g]	11.3 – 12.6[a]
Ge (diamond→ β-tin)	6.6	7.9	11.3	9.8[l]	10.6(5)[b]
Sn (β-tin→ bct)	10.3	5.4	16.2	19[h], 10.4[i]	9.5[c], 13[m], 15 – 20[n]
Pb (fcc → hcp)	11.6	13.9	16	13[j]	14[d]
SiC (zb → NaCl)	59.4	64.8	74	67[k]	35|100[e]

[a]Reference [24].
[b]Reference [25].
[c]Reference [26].
[d]Reference [27].
[e]Reference [28].
[f]Reference [2].
[g]Reference [4].
[h]Reference [29].
[i]Reference [30].
[j]Reference [31].
[k]Reference [32].
[l]Reference [33].
[m]Reference [30].
[n]Reference [34].

bonding of the low- and high-pressure phases and properly stabilize the covalent single bond.

The transition pressure for Ge is 10.6 GPa [25]. Taking ZPE and finite temperature correction [35] into account, LDA predicts a transition pressure of 5.9 GPa, PBE gives 7.5 GPa, and SCAN gives 10.1 GPa, in excellent agreement with experimental results.

B. Sn

Tin crystallizes in the β phase (white tin) at normal temperature and pressure. On application of pressure, the β phase undergoes a transition to the body-centered tetragonal (bct) phase at about 9.5 GPa [26] at room temperature. At 0 K, the transition pressure is estimated to be about 15–20 [34] or 13 GPa [30] from the measured equation of state. The calculation with LDA gives a pressure of 10.3 GPa, close to the experimental pressure at room temperature. It also agrees with the pressure reported by Ref. [30]. However, the SCAN result (16.2 GPa) is in agreement with the experimental transition pressure of Ref. [34] at 0 K. PBE underestimates the transition pressure.

C. Pb

The tetrahedrally bonded structure is completely absent in Pb. It crystallizes in the fcc structure. It undergoes a transition to the hexagonal close-packed structure at 14 GPa [27]. LDA predicts a smaller transition pressure of 11.6 GPa, while PBE predicts 13.9 GPa, and SCAN predicts 16 GPa, in agreement with experimental results.

D. SiC

SiC undergoes a phase transition from the 3C-SiC polytype form to the NaCl structure at about 100 GPa [28]. The high-pressure phase persists until 35 GPa under decompression, indicating a very large hysteresis. The predictions of LDA, PBE, and SCAN fall within the experimental error bar.

E. GaP

Gallium phosphide is a wide band-gap semiconductor. It crystallizes in the zinc-blende (zb) structure at ambient conditions. The high-pressure phase of GaP was initially reported to be the tetragonal β-Sn structure by x-ray diffraction experiments [36,37]. However, Nelmes *et al*. [38] showed that only a distorted Cmcm structure is compatible with the observed angle-dispersive x-ray (ADX) powder diffraction pattern and also with the Ruoff x-ray pattern, ruling out the existence of the β-tin structure. Mujica *et al*. [52] studied the high-pressure phases of GaP with a density functional calculation within LDA. They found the coexistence pressure for the zinc-blende and Cmcm phases as 17.7 GPa. Our calculation with LDA predicts a pressure of 18.1 GPa, low compared to the experimental value of 26 GPa [38]. PBE gives a better pressure of 20.7 GPa. SCAN predicts a transition pressure of 25.9 GPa, in excellent agreement with experimental results.

F. GaAs

GaAs is an important semiconductor for its technological uses in solar cells, semiconductor lasers, diodes, etc. At about 17 GPa, it was initially reported to undergo a phase transition from the zinc-blende structure to an orthorhombic structure with space group *Pmm*2 [39]. But, later the high-pressure phase was confimed to be a structure having space group *Cmcm* [40]. Theoretical study [53] on the stability of high-pressure phases of GaAs showed that the Cmcm structure is indeed favored over other reported candidates like NaCl, Pmm2 structure. Our calculations using LDA and PBE predict a lower pressure such as 12.4 and 14.1 GPa, respectively, low in comparison

TABLE II. The calculated equlibrium transition pressure (in GPa) for the group III-IV compounds within the LDA, PBE, and SCAN XC functionals. ZPE and vibrational effects are not included in the calculated value. The experimental pressure (in GPa) to the right of the vertical bar corresponds to forward transition and the left one to reverse transition.

	LDA	PBE	SCAN	Other work	Expt.
GaP (zb → Cmcm)	18.1	20.7	25.9	17.7[o]	26[a]
GaAs (zb → Cmcm)	12.4	14.1	17.1	12.1[p]	11.2|17.3[b]
GaN (wur → NaCl)	42.3	46.2	42.1	42.5[r], 33.7[q]	30|47[f], 52.2[g], 37[h]
InN (wur → NaCl)	8.9	12.2	10.6	10[q]	12.1[g], 10[i]
AlN (wur → NaCl)	7.2	13.1	12.5	9.2[q]	0|14[c], 22[d], 20[e]
InP (zb → NaCl)	6.2	8.4	10.6	5.6[o], 7.4[t]	9.8(5)[j], 10.8(5)[k]
InAs (zb → NaCl)	4.2	6.0	7.5	3.9[o]	7.0[l],
AlP (zb → NiAs)	6.8	9.4	11.5	7.7[s]	4.8|14.2[m]
AlAs (zb → NiAs)	6.7	8.9	10.7	7[s]	2|12[n]
AlSb (zb → Cmcm)	3.7	5.1	6.6	4.7[s]	2.2|8.1[a]

[a]Reference [38].
[b]Reference [40].
[c]Reference [41].
[d]Reference [42].
[e]Reference [43].
[f]Reference [44].
[g]Reference [45].
[h]Reference [46].
[i]Reference [47].
[j]Reference [1].
[k]Reference [48].
[l]Reference [49].
[m]Reference [50].
[n]Reference [51].
[o]Reference [52].
[p]Reference [53].
[q]Reference [54].
[r]Reference [55].
[s]Reference [56].
[t]Reference [57].

to experimental results. SCAN gives a transition pressure of 17.1 GPa, in agreement with experimental results.

Although experiments and theoretical studies have shown that GaAs-II is the Cmcm structure, a recent QMC study [58] has investigated the zb → NaCl transition. QMC predicts 17 GPa for this semiconductor-metal transition, so we have also made calculations for this transition. Both LDA (12.7 GPa) and PBE (14.6 GPa) underestimate the transition pressure, while the SCAN result (18.7 GPa) is in good agreement with the QMC value. Furthermore, our results for this transition pressure are higher than that for zb → Cmcm, indicating that the zb → Cmcm transition is energetically favored over the zb → NaCl transition.

G. GaN, InN, and AlN

GaN, AlN, and InN crystallize in the wurtzite structure at ambient conditions. However, they can also be modified into the zinc-blende structure using an epitaxial technique. The wurtzite phase has a wide band gap, so it is useful for optoelectronic devices that operate in high-frequency ranges. On application of pressure, the wurtzite phase undergoes a transition to the NaCl phase.

For AlN, the experimental phase transition has been reported to occur at 22.9 GPa by Ueno *et al.* [42], at 14 GPa by Xia *et al.* [41], and at 20 GPa by Uehara *et al.* [43]. Xia *et al.* also observed that the high-pressure phase stays in the NaCl structure down to atmospheric pressure, indicating a large hysteresis. Our calculation with LDA gives a transition pressure of 7.2 GPa, PBE gives 13.1 GPa, and SCAN predicts 12.5 GPa. Taking the uncertainty due to the hysteresis into account, our results are close to the middle of the hysteresis cycle.

Different values for transition pressure have been reported for GaN as well. Xia *et al.* [46] using an EDX method reported 37 GPa, while Ueno *et al.* [45] (ADX method) found 52.2 GPa. Another experiment [44] reported a forward transition pressure of 47 GPa and 30 GPa upon decompression. Our calculation with LDA predicts a pressure of 42.3 GPa, PBE predicts 46.2 GPa, and SCAN predicts 42.1 GPa. All calculated pressures are in agreement with experimental results within the reported experimental values 37–52.2 GPa. Interestingly, the LDA pressure is here similar to SCAN and RPA results (42.5 GPa) [55], and is higher than the LDA value reported by Serrano *et al.* [54].

For InN, Xia *et al.* [47] found the transition to occur at 10 GPa and the reverse transition at 5 GPa, while Ueno *et al.* [45] reported the transition pressure as 12.1 GPa. Our calculated transition pressures are 8.9 GPa (LDA), 12.2 GPa (PBE), and 10.6 GPa (SCAN), in reasonable agreement with experimental results.

TABLE III. The calculated equilibrium transition pressure (in GPa) for the group II-VI materials within the LDA, PBE, and SCAN XC functionals. ZPE and vibrational effects are not included in the calculated value. The experimental pressure (in GPa) to the right of the vertical bar corresponds to the forward transition and the left one to the reverse transition.

	LDA	PBE	SCAN	Other work	Expt.
ZnO (wur → NaCl)	9.1	11.6	8.8	6.6[q], 9.3[q], 9.18[r]	1.9(2)|9.1(2)[a], 9.8[b]
ZnS (zb → NaCl)	15.2	16.8	18.3	14.35[s], 15.4[t], 17.2[u]	10|14.7[c], 17.4[d], 16.9[e]
ZnSe (zb → NaCl)	12.1	13.7	15.9	15.2[f], 11[v], 14.7[u]	12 − 20[f]
ZnTe (zb → cinn)	8.7	9.7	10.5	10.3[u]	8|9.5[g]
CdS (wur → NaCl)	2.4	4.4	2.9	3.1[w]	1.2|2.54[h], 3[i]
CdSe (wur → NaCl)	2.4	4.1	3.3	2.5[v]	1.7|2.72[j]
CdTe (zb → cinn)	3.8	4.8	4.2	2.5[v]	2.67|3.53[k], 3.8[l]
HgS (cinn → NaCl)	11.1	15.8	21.9	26.57[x]	20.5(7)[m]
HgSe (cinn → NaCl)	6.7	10.4	15.8	7[y], 11.5[y]	14.6(6)[n], 15.5[o]
HgTe (cinn → NaCl)	2.3	5.2	6.6	2.5[y], 6.5[y]	8[p,o]

[a]Reference [59].
[b]Reference [60].
[c]Reference [61].
[d]Reference [62].
[e]Reference [63].
[f]Reference [64,65].
[g]Reference [66].
[h]Reference [67].
[i]Reference [68].
[j]Reference [69].
[k]Reference [70].
[l]Reference [71].
[m]Reference [72].
[n]Reference [73].
[o]Reference [74].
[p]Reference [75].
[q]Reference [76].
[r]Reference [55].
[s]Reference [77].
[t]Reference [78].
[u]Reference [79].
[v]Reference [80].
[w]Reference [81].
[x]Reference [82].
[y]Reference [83].

H. InP and InAs

InP and InAs crystallize in the zinc-blende structure at normal conditions. The first transition is from zinc-blende to the NaCl structure. The transition pressure for InP is 9.8 GPa [1], or 10.8 ± 0.05 GPa [48]. Our calculated pressures with LDA (6.2 GPa) and PBE (8.4 GPa) are smaller than the experimental results. SCAN predicts the transition pressure as 10.6 GPa, in good agreement with experiments.

The transition of InAs occurs at 7 GPa [49,84]. LDA predicts the transition to occur at 4.2 GPa. The PBE prediction (6 GPa) is close to experiment, while the SCAN result (7.5 GPa) is in better agreement with experimental results.

I. AlP and AlAs

AlP and AlAs crystallize in the zinc-blende structure at normal conditions. On application of pressure, they were found to transform to a metallic phase: the NiAs structure. The NiAs phase for AlAs was first predicted theoretically by Froyen *et al*. [85] before it was verified experimentally by Greene *et al*. [51].

For AlAs, the transition is found to occur at 12 GPa [51], while the reverse transition occurs at 2 GPa. Our calculated pressure with LDA, PBE, and SCAN are well within 2–12 GPa (Table II).

The transition of AlP was reported to occur between 4.8 and 14.2 GPa [50]. The pressure with LDA is 6.8 GPa, small compared to the middle of the hysteresis interval (9.5 GPa). PBE and SCAN predict 9.4 and 11.5 GPa, respectively, and are in better agreement with the experimental results.

J. AlSb

The low-pressure phase of AlSb is the zinc-blende structure. Different structures were assigned as the high-pressure phase until Nelmes *et al*. [38] identified it as an orthorhombic structure with space group *Cmcm*. A theoretical study of Mujica *et al*. [56] also shows that the transition to the Cmcm structure is favored over the zb → NiAs transition, as in AlP

and AlAs. The transition was reported to occur at 8.1 GPa [38] with a hysteresis [86]. Our calculated pressure for the zb → Cmcm transition with LDA is underestimated, while PBE and SCAN are in reasonable agreement with experiment (Table II).

K. ZnO

ZnO undergoes a transition from its low-pressure wurtzite structure to the semiconducting NaCl structure at 9.8 GPa [60] or at 9.1 GPa [59], with a large hysteresis. Our LDA pressure (9.1 GPa) is higher than that reported by Jaffe *et al.* [76]. The LDA, PBE, and SCAN results are close to the onset of the transition on an increase of pressure. The LDA and SCAN pressures are also in agreement with the RPA result (9.18 GPa) [55].

L. ZnS

ZnS crystallizes in the zinc-blende structure at ambient pressure. On application of pressure, it transforms to the NaCl structure at 17.4 ± 1.2 GPa [62] or at 14.7 GPa [87]. However, a more recent experiment [63] reports the pressure as 16.9 GPa. The calculated pressures with LDA, PBE, and SCAN are within the experimental range 15 to 17.4 GPa.

M. ZnSe

ZnSe undergoes a phase transition from zinc-blende to the metallic NaCl structure at about 12–20 GPa [64]. Galit *et al.* [65] have reported that ZnSe undergoes a transition to a narrow-gap semiconducting phase [88] and to the metallic NaCl phase at 17 GPa. The low-pressure phase was recovered at 10.5 GPa under decompression. For the zb → NaCl transition, our results with LDA (12.1 GPa), PBE (13.7 GPa), and SCAN (15.9 GPa) are in reasonable agreement with experimental results.

N. ZnTe

Unlike ZnS and ZnSe, ZnTe undergoes a transition to the semiconducting trigonal cinnabar structure. The transition pressure is about 9.5 GPa [66]. Our calculations with LDA (8.7 GPa), PBE (9.7 GPa), and SCAN (10.5 GPa) are in agreement with experimental results.

O. CdS and CdSe

Both CdS and CdSe have the wurtzite structure under normal conditions. They undergo a wurtzite to NaCl transition on the application of pressure 2–3 GPa. For CdS, the transition is reported to occur at 2.54 [67] or 3 GPa [68]. The transition pressure with LDA is 2.4 GPa, smaller than the experimental pressure. PBE predicts a higher transition pressure. SCAN is in excellent agreement with experimental results.

For CdSe, the transition pressure is 2.72 GPa [69]. The calculated pressure with LDA is 2.3 GPa. PBE predicts a higher pressure, while the SCAN result (3.2 GPa) is in excellent agreement with the experimental results.

P. CdTe

Although there was an initial report of a zb → NaCl transition at 3.53 GPa [70], Nelmes *et al.* [89] found an intermediate trigonal cinnabar phase with a transition pressure at 3.5 GPa. Using the electrical resistivity method, a recent experiment reports the transition pressure as 3.8 GPa [71]. The calculated pressures with LDA, PBE, and SCAN are in reasonably good agreement with the experimental results.

Q. HgS

HgS crystallizes in the cinnabar structure at normal conditions. On application of pressure, it undergoes a structural transition to the NaCl structure at 20.5 GPa [72]. Both LDA and PBE underestimate the transition pressure, while SCAN is in excellent agreement with experimental results.

R. HgSe and HgTe

A theoretical study [83] by Mujica *et al.* has shown that LDA and PBE work well for the first transition (zb to cinn), and underestimate pressure for the cinn → NaCl transition. Our LDA and PBE results (except PBE result for HgTe, which is smaller in our case) agree with their results. SCAN is in better agreement with experimental results.

IV. OVERALL ANALYSIS

Figure 1 and Table IV compare the predictions of the XC functionals LDA, PBE, and SCAN to experimental results. Except for a few materials, LDA underestimates the coexistence pressure, in agreement with the conclusions of Mujica *et al.* [1]. PBE improves upon the LDA prediction, but it still underestimates the pressure in many cases and overestimates in a few. On the other hand, SCAN predictions are in good agreement with the experimental transition pressures.

The predictive power of density functionals in the present context depends upon how well they capture the energy

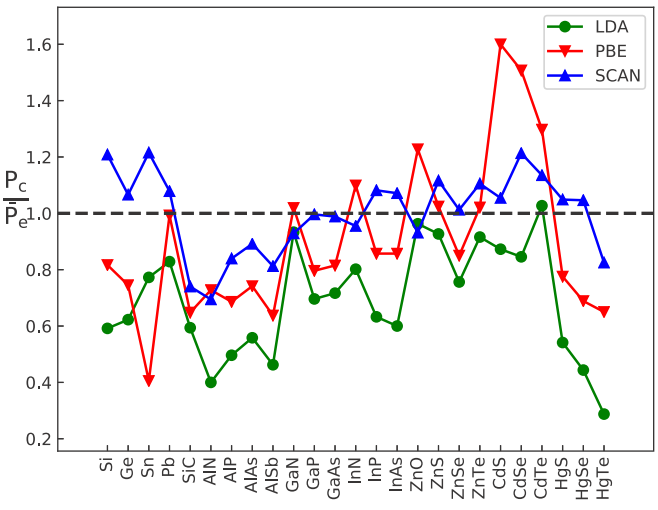

FIG. 1. Ratio of the calculated transition pressure P_c and the experimental pressure $\bar{P}_e$. $\bar{P}_e$ is the average of all experimental forward pressures (from Tables I–III). An accurate functional might make this ratio less than or about equal to 1, in view of hysteresis, uncertainty, and vibrational effects in the experiments. Reverse pressures have been measured for only 13 out of the 25 materials.

TABLE IV. The mean percentage error (MPE) and mean absolute percentage error (MAPE) for XC functionals LDA, PBE, and SCAN. The experimental reference value is $\tilde{P}_e$, as defined in the caption of Fig. 1.

	LDA	PBE	SCAN
MPE	−30.92	−10.17	0.36
MAPE	31.14	24.54	11.78

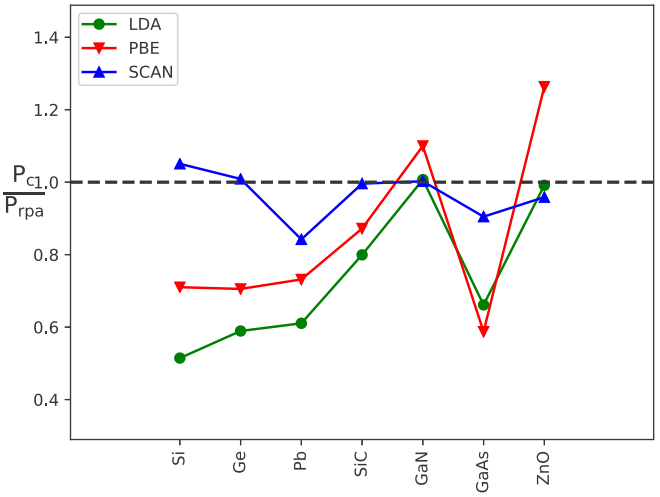

FIG. 2. Comparison of the calculated transition pressure P_c with the RPA transition pressure P_{rpa}.

difference of the two phases. The systematic underestimation by LDA can be understood by the fact that it favors homogeneity. Since the high-pressure phases are more closely packed structures, their electron density is somewhat more homogeneous. As a result, LDA works better for the high-pressure phase than it does for the low-pressure phase, thereby underestimating the true energy difference. The better PBE results are due to an improved energy difference. PBE lowers the total energy of the more inhomogeneous phase more and thus increases the difference. The ability of SCAN to predict an accurate transition pressure is due to its better description of diverse kinds of bonding, including the covalent bonding in diamond-structure Si and Ge.

It has been argued that the inaccurate prediction of transition pressure by semilocal functionals is due to their inaccurate description of the band gap. The HSE06 functional gives the correct transition pressure for the diamond to β-tin transition for silicon, and also gives an accurate band gap. However, our calculation shows that SCAN gives an accurate transition pressure although it only partly improves the band gap [13], calling the relevance of the gap into question.

It is important to remark that we have neglected the zero-point motion of ions and the effect of temperature in our calculations. Most of the experimental pressures are measured at room temperature, whereas the calculated pressures correspond to 0K. This makes the comparison of the experiment and theory difficult. However, in the case of Si and Ge, inclusion of these effects makes the performance of SCAN even better. The temperature dependence [30,34] in the case of Sn explains in part the apparent overestimation of the pressure within SCAN. We expect the agreement between experiment and the SCAN results to be good for other materials as well.

Hysteresis can also be a major issue in the comparison. The kinetic barrier between two coexisting phase often hinders the transition, leading to the hysteresis. This makes it hard to locate the true equilibrium transition point experimentally. The middle of the hysteresis cycle is sometimes taken as an estimate of the equilibrium transition pressure, and half the width of the cycle as its uncertainty.

Because of all these uncertainties, our fixed-nucleus equilibrium transition pressures can be more cleanly compared to those of a fifth-rung density functional, the random phase approximation or RPA in a density functional context [90], also implemented for calculation of the equilibrium transition pressure at fixed nuclear positions. Figure 2 shows this comparison for our seven materials for which an RPA transition pressure is known [55,91] and suggests an almost systematic improvement as we climb the ladder from LDA to PBE to SCAN to RPA. For isoelectronic energy differences [16,91–94] in condensed matter, for which RPA is typically accurate, SCAN results are often close to those of the expensive RPA. For the materials where QMC equlibrium transition pressures are known, SCAN is close to QMC (with a 6% difference for Si diamond → β-tin and 10% for GaAs zb → NaCl).

The clearest and most dramatic message from Fig. 2 is the great improvement from LDA to PBE to SCAN for the equilibrium transition pressures of the covalent semiconductor-metal transitions (e.g., Si and Ge), due to an increasing relative stabilization of the covalent semiconducting phase under increasing functional sophistication. Specifically, the PBE enhancement factor over LDA exchange increases above one as the magnitude of the local density gradient increases, stabilizing the more inhomogeneous phase. The SCAN enhancement factor over LDA exchange is greater than one even at bond centers where the density gradient is zero, so long as the variable α defined in Sec. I is close to zero there, and this further stabilizes covalent bonds. In contrast, "GGAs for solids," such as AM05 [95] and PBEsol [96] yield better lattice constants and bulk moduli than LDA or PBE, and better surface energies [14] than PBE, but can be worse [2] than both for the transition pressure in Si.

PBE includes almost no van der Waals (vdW) attraction, AM05 and PBEsol provide an intermediate-range vdW correction to PBE, which as expected stabilizes preferentially the higher density phase and so reduces the transition pressure. While SCAN includes intermediate-range vdW [6,14], it also includes other effects (i.e., recognizes different chemical environments characterized by different chemical bonds) which raise the transition pressure in 19 of the 25 cases studied here.

Just as SCAN halves the PBE mean absolute error for the transition pressures in Table IV, it does the same [15,97] for the formation energies of solids and for their predicted ground-state crystal structures. In a recent and very extensive test for main-group molecules [98] the nonempirical SCAN outperformed all other tested meta-GGAs, including those heavily fitted to molecular data. Molecules have much in common with semiconductors.

V. CONCLUSIONS

We have investigated the performance of the nonempirical, general-purpose, semilocal density functionals LDA, PBE, and SCAN for the first structural phase transitions of 25 group IV, III-V, and II-VI compounds. LDA underestimates the transition pressures, while PBE can under- or overestimate. SCAN provides a systematic improvement over LDA and PBE, and its predictions are in reasonable agreement with experimental results. For those materials where a comparison can be made, SCAN yields transition pressures as good as computationally more expensive methods like the hybrid functional HSE06, RPA, and QMC. We conclude that SCAN is a usefully accurate and efficient method for predicting transition pressures in these and probably other solids. For tests on some other solids, see Ref. [91].

ACKNOWLEDGMENTS

We thank Haowei Peng, Jefferson E. Bates, Christopher R. Spano, Yubo Zhang, Abhirup Patra, Niraj Nepal, and Niladri Sengupta for their help during calculations. This work was supported by National Science Foundation under Grant No. DMR-1607868. This research was supported in part by the National Science Foundation through major research instrumentation Grant No. CNS-09-58854. J.S. acknowledges the support from the Center for Computational Design of Functional Layered Materials, an Energy Frontier Research Center funded by the US Department of Energy (DOE), Office of Science, Basic Energy Sciences (BES) under Award No. DE-SC0012575. The figures were generated by MATPLOTLIB [99]. AFLOW software [100] was used to create the primitive cell.

C.S., J.S., and J.P.P. designed the project and wrote the paper, while C.S. performed all the calculations.

[1] A. Mujica, A. Rubio, A. Muñoz, and R. J. Needs, Rev. Mod. Phys. **75**, 863 (2003).
[2] R. G. Hennig, A. Wadehra, K. P. Driver, W. D. Parker, C. J. Umrigar, and J. W. Wilkins, Phys. Rev. B **82**, 014101 (2010).
[3] E. R. Batista, J. Heyd, R. G. Hennig, B. P. Uberuaga, R. L. Martin, G. E. Scuseria, C. J. Umrigar, and J. W. Wilkins, Phys. Rev. B **74**, 121102 (2006).
[4] B. Xiao, J. Sun, A. Ruzsinszky, J. Feng, R. Haunschild, G. E. Scuseria, and J. P. Perdew, Phys. Rev. B **88**, 184103 (2013).
[5] J. Sun, A. Ruzsinszky, and J. P. Perdew, Phys. Rev. Lett. **115**, 036402 (2015).
[6] J. Sun, R. C. Remsing, Y. Zhang, Z. Sun, A. Ruzsinszky, H. Peng, Z. Yang, A. Paul, U. Waghmare, X. Wu, M. L. Klein, and J. P. Perdew, Nat. Chem. **8**, 831 (2016).
[7] W. Kohn and L. J. Sham, Phys. Rev. **140**, A1133 (1965).
[8] J. P. Perdew and S. Kurth, in *A Primer for Density functional Theory*, edited by C. Fiolhais, F. Nogueira, and M. Marques, Lecture Notes in Physics, Vol. 620 (Springer, Berlin, 2003), Chap. 1.
[9] J. P. Perdew and K. Schmidt, AIP Conf. Proc. **577**, 1 (2001).
[10] J. P. Perdew, K. Burke, and M. Ernzerhof, Phys. Rev. Lett. **77**, 3865 (1996).
[11] J. Sun, B. Xiao, Y. Fang, R. Haunschild, P. Hao, A. Ruzsinszky, G. I. Csonka, G. E. Scuseria, and J. P. Perdew, Phy. Rev. Lett. **111**, 106401 (2013).
[12] A. Paul, J. Sun, J. P. Perdew, and U. V. Waghmare, Phys. Rev. B **95**, 054111 (2017).
[13] Z.-H. Yang, H. Peng, J. Sun, and J. P. Perdew, Phys. Rev. B **93**, 205205 (2016).
[14] A. Patra, J. E. Bates, J. Sun, and J. P. Perdew, Proc. Natl. Acad. Sci. USA **114**, E9188 (2017).
[15] Y. Zhang, D. A. Kitchaev, J. Yang, T. Chen, S. T. Dacek, R. A. Sarmiento-Pérez, M. Marques, H. Peng, G. Ceder, J. P. Perdew, and J. Sun [npj Comput. Mater. (to be published)].
[16] M. Chen, H.-Y. Ko, R. C. Remsing, M. F. C. Andrade, B. Santra, Z. Sun, A. Selloni, R. Car, M. L. Klein, J. P. Perdew, and X. Wu, Proc. Natl. Acad. Sci. USA **114**, 10846 (2017).
[17] R. C. Remsing, M. L. Klein, and J. Sun, Phys. Rev. B **96**, 024203 (2017).
[18] G. Kresse and J. Furthmüller, Phys. Rev. B **54**, 11169 (1996).
[19] G. Kresse and D. Joubert, Phys. Rev. B **59**, 1758 (1999).
[20] D. M. Ceperley and B. J. Alder, Phys. Rev. Lett. **45**, 566 (1980).
[21] J. P. Perdew and A. Zunger, Phys. Rev. B **23**, 5048 (1981).
[22] See Supplemental Material at http://link.aps.org/supplemental/10.1103/PhysRevB.97.094111 for more details about the integration grid sizes and kinetic energy cutoffs for the energy-volume calculations and the fit parameters for the energy-volume curves.
[23] F. Murnaghan, Proc. Natl. Acad. Sci. USA **30**, 244 (1944).
[24] J. Z. Hu, L. D. Merkle, C. S. Menoni, and I. L. Spain, Phys. Rev. B **34**, 4679 (1986).
[25] C. S. Menoni, J. Z. Hu, and I. L. Spain, Phys. Rev. B **34**, 362 (1986).
[26] H. Olijnyk and W. B. Holzapfel, J. Physique (Paris) Colloq. **45**, C8 (1984).
[27] H. Mao, Y. Wu, J. Shu, J. Hu, R. Hemley, and D. Cox, Solid State Commun. **74**, 1027 (1990).
[28] M. Yoshida, A. Onodera, M. Ueno, K. Takemura, and O. Shimomura, Phys. Rev. B **48**, 10587 (1993).
[29] B. H. Cheong and K. J. Chang, Phys. Rev. B **44**, 4103 (1991).
[30] N. E. Christensen and M. Methfessel, Phys. Rev. B **48**, 5797 (1993).
[31] A. Y. Liu, A. García, M. L. Cohen, B. K. Godwal, and R. Jeanloz, Phys. Rev. B **43**, 1795 (1991).
[32] K. Karch, F. Bechstedt, P. Pavone, and D. Strauch, Phys. Rev. B **53**, 13400 (1996).
[33] N. Moll, M. Bockstedte, M. Fuchs, E. Pehlke, and M. Scheffler, Phys. Rev. B **52**, 2550 (1995).
[34] J. L. Corkill, A. García, and M. L. Cohen, Phys. Rev. B **43**, 9251 (1991).
[35] K. Gaál-Nagy, A. Bauer, M. Schmitt, K. Karch, P. Pavone, and D. Strauch, Phys. Stat. Solidi B **211**, 275 (1999).
[36] M. Baublitz, Jr. and A. L. Ruoff, J. Appl. Phys. **53**, 6179 (1982).
[37] J. Z. Hu, D. R. Black, and I. L. Spain, Solid State Commun. **51**, 285 (1984).
[38] R. J. Nelmes, M. I. McMahon, and S. A. Belmonte, Phys. Rev. Lett. **79**, 3668 (1997).

[39] S. T. Weir, Y. K. Vohra, C. A. Vanderborgh, and A. L. Ruoff, Phys. Rev. B **39**, 1280 (1989).
[40] M. I. McMahon and R. J. Nelmes, Phys. Rev. Lett. **78**, 3697 (1997).
[41] Q. Xia, H. Xia, and A. L. Ruoff, J. Appl. Phys. **73**, 8198 (1993).
[42] M. Ueno, A. Onodera, O. Shimomura, and K. Takemura, Phys. Rev. B **45**, 10123 (1992).
[43] S. Uehara, T. Masamoto, A. Onodera, M. Ueno, O. Shimomura, and K. Takemura, J. Phys. Chem. Solids **58**, 2093 (1997).
[44] P. Perlin, C. Jauberthie-Carillon, J. P. Itié, A. San Miguel, I. Grzegory, and A. Polian, Phys. Rev. B **45**, 83 (1992).
[45] M. Ueno, M. Yoshida, A. Onodera, O. Shimomura, and K. Takemura, Phys. Rev. B **49**, 14 (1994).
[46] H. Xia, Q. Xia, and A. L. Ruoff, Phys. Rev. B **47**, 12925 (1993).
[47] Q. Xia, H. Xia, and A. L. Ruoff, Mod. Phys. Lett. B **08**, 345 (1994).
[48] C. S. Menoni and I. L. Spain, Phys. Rev. B **35**, 7520 (1987).
[49] R. J. Nelmes, M. I. McMahon, N. G. Wright, D. R. Allan, H. Liu, and J. S. Loveday, J. Phys. Chem. Solids **56**, 539 (1995).
[50] R. G. Greene, H. Luo, and A. L. Ruoff, J. Appl. Phys. **76**, 7296 (1994).
[51] R. G. Greene, H. Luo, T. Li, and A. L. Ruoff, Phys. Rev. Lett. **72**, 2045 (1994).
[52] A. Mujica and R. J. Needs, Phys. Rev. B **55**, 9659 (1997).
[53] A. Mujica and R. J. Needs, J. Phys. Condens. Matter **8**, L237 (1996).
[54] J. Serrano, A. Rubio, E. Hernández, A. Muñoz, and A. Mujica, Phys. Rev. B **62**, 16612 (2000).
[55] H. Peng and S. Lany, Phys. Rev. B **87**, 174113 (2013).
[56] A. Mujica, P. Rodríguez-Hernández, S. Radescu, R. J. Needs, and A. Muñoz, Phys. Stat. Solidi B **211**, 39 (1999).
[57] O. Arbouche, B. Belgoumène, B. Soudini, Y. Azzaz, H. Bendaoud, and K. Amara, Comput. Mater. Sci. **47**, 685 (2010).
[58] C. N. M. Ouma, M. Z. Mapelu, N. W. Makau, G. O. Amolo, and R. Maezono, Phys. Rev. B **86**, 104115 (2012).
[59] S. Desgreniers, Phys. Rev. B **58**, 14102 (1998).
[60] F. Decremps, J. Zhang, and R. C. Liebermann, EPL **51**, 268 (2000).
[61] H. Karzel, W. Potzel, M. Köfferlein, W. Schiessl, M. Steiner, U. Hiller, G. M. Kalvius, D. W. Mitchell, T. P. Das, P. Blaha, K. Schwarz, and M. P. Pasternak, Phys. Rev. B **53**, 11425 (1996).
[62] W. H. Gust, J. Appl. Phys. **53**, 4843 (1982).
[63] J. Yang, F. Zhu, Q. Zhang, Y. Wu, X. Wu, S. Qin, J.-C. Dong, and D.-L. Chen, Chin. Phys. Lett. **30**, 046101 (2013).
[64] V. I. Smelyansky and J. S. Tse, Phys. Rev. B **52**, 4658 (1995).
[65] G. Itkin, G. R. Hearne, E. Sterer, M. P. Pasternak, and W. Potzel, Phys. Rev. B **51**, 3195 (1995).
[66] A. San-Miguel, A. Polian, M. Gauthier, and J. P. Itié, Phys. Rev. B **48**, 8683 (1993).
[67] H. Sowa, Solid State Sci **7**, 73 (2005).
[68] Y. Li, X. Zhang, H. Li, X. Li, C. Lin, W. Xiao, and J. Liu, J. Appl. Phys. **113**, 083509 (2013).
[69] H. Sowa, Solid State Sci **7**, 1384 (2005).
[70] A. N. Mariano and E. P. Warekois, Science **142**, 672 (1963).
[71] C. He, C. X. Gao, B. G. Liu, M. Li, X. W. Huang, A. M. Hao, C. L. Yu, D. M. Zhang, Y. Wang, H. W. Liu, Y. Z. Ma, and Z. T. Zou, J. Phys. Condens. Matter **19**, 425223 (2007).
[72] R. J. Nelmes and M. I. McMahon, *Semiconductors and Semimetals* (Academic Press, New York, 1998), Chap. 3, pp. 145–246.
[73] M. I. McMahon, R. J. Nelmes, H. Liu, and S. A. Belmonte, Phys. Rev. Lett. **77**, 1781 (1996).
[74] A. Ohtani, T. Seike, M. Motobayashi, and A. Onodera, J. Phys. Chem. Solids **43**, 627 (1982).
[75] A. San-Miguel, N. G. Wright, M. I. McMahon, and R. J. Nelmes, Phys. Rev. B **51**, 8731 (1995).
[76] J. E. Jaffe, J. A. Snyder, Z. Lin, and A. C. Hess, Phys. Rev. B **62**, 1660 (2000).
[77] A. Qteish, M. Abu-Jafar, and A. Nazzal, J. Phys. Condens. Matter **10**, 5069 (1998).
[78] X.-R. Chen, X.-F. Li, L.-C. Cai, and J. Zhu, Solid State Commun. **139**, 246 (2006).
[79] J. J. Tan, G. F. Ji, X. R. Chen, and Q. Q. Gou, Commun. Theor. Phys. **53**, 1160 (2010).
[80] M. Côté, O. Zakharov, A. Rubio, and M. L. Cohen, Phys. Rev. B **55**, 13025 (1997).
[81] M. D. Knudson, Y. M. Gupta, and A. B. Kunz, Phys. Rev. B **59**, 11704 (1999).
[82] S. R. Sun and Y. H. Dong, Phys. Rev. B **72**, 174101 (2005).
[83] S. Radescu, A. Mujica, J. López-Solano, and R. J. Needs, Phys. Rev. B **83**, 094107 (2011).
[84] Y. K. Vohra, S. T. Weir, and A. L. Ruoff, Phys. Rev. B **31**, 7344 (1985).
[85] S. Froyen and M. L. Cohen, Phys. Rev. B **28**, 3258 (1983).
[86] R. G. Greene, H. Luo, K. Ghandehari, and A. L. Ruoff, J. Phys. Chem. Solids **56**, 517 (1995).
[87] Y. Zhou, A. J. Campbell, and D. L. Heinz, J. Phys. Chem. Solids **52**, 821 (1991).
[88] S. Cui, H. Hu, W. Feng, X. Chen, and Z. Feng, J. Alloys Compd. **472**, 294 (2009).
[89] R. J. Nelmes, M. I. McMahon, N. G. Wright, and D. R. Allan, Phys. Rev. B **48**, 1314 (1993).
[90] D. C. Langreth and J. P. Perdew, Phys. Rev. B **21**, 5469 (1980).
[91] N. Sengupta, J. E. Bates, and A. Ruzsinszky (unpublished).
[92] M. Bokdam, J. Lahnsteiner, B. Ramberger, T. Schäfer, and G. Kresse, Phys. Rev. Lett. **119**, 145501 (2017).
[93] N. K. Nepal, J. E. Bates, and A. Ruzsinszky [Phys. Rev. B (to be published)].
[94] H. Peng, Z.-H. Yang, J. P. Perdew, and J. Sun, Phys. Rev. X **6**, 041005 (2016).
[95] R. Armiento and A. E. Mattsson, Phys. Rev. B **72**, 085108 (2005).
[96] J. P. Perdew, A. Ruzsinszky, G. I. Csonka, O. A. Vydrov, G. E. Scuseria, L. A. Constantin, X. Zhou, and K. Burke, Phys. Rev. Lett. **100**, 136406 (2008).
[97] Y. Hinuma, H. Hayashi, Y. Kumagai, I. Tanaka, and F. Oba, Phys. Rev. B **96**, 094102 (2017).
[98] L. Goerigk, A. Hansen, C. Bauer, S. Ehrlich, A. Najibi, and S. Grimme, Phys. Chem. Chem. Phys. **19**, 32184 (2017).
[99] J. D. Hunter, Comput. Sci. Eng. **9**, 90 (2007).
[100] S. Curtarolo, W. Setyawan, G. L. Hart, M. Jahnatek, R. V. Chepulskii, R. H. Taylor, S. Wang, J. Xue, K. Yang, O. Levy *et al.*, Comput. Mater. Sci. **58**, 218 (2012).